

# ASAP: Architecture Search, Anneal and Prune

Asaf Noy<sup>1</sup>, Niv Nayman<sup>1</sup>, Tal Ridnik<sup>1</sup>, Nadav Zamir<sup>1</sup>, Sivan Doveh<sup>2</sup>,  
Itamar Friedman<sup>1</sup>, Raja Giryes<sup>2</sup>, and Lihi Zelnik-Manor<sup>1</sup>

<sup>1</sup>DAMO Academy, Alibaba Group (first.last@alibaba-inc.com)

<sup>2</sup>School of Electrical Engineering, Tel-Aviv University Tel-Aviv, Israel

## Abstract

*Automatic methods for Neural Architecture Search (NAS) have been shown to produce state-of-the-art network models, yet, their main drawback is the computational complexity of the search process. As some primal methods optimized over a discrete search space, thousands of days of GPU were required for convergence. A recent approach is based on constructing a differentiable search space that enables gradient-based optimization, thus reducing the search time to a few days. While successful, such methods still include some incontinuous steps, e.g., the pruning of many weak connections at once. In this paper, we propose a differentiable search space that allows the annealing of architecture weights, while gradually pruning inferior operations, thus the search converges to a single output network in a continuous manner. Experiments on several vision datasets demonstrate the effectiveness of our method with respect to the search cost, accuracy and the memory footprint of the achieved model.*

## 1. Introduction

Over the last few years deep neural networks highly succeed in computer vision tasks, mainly because of their automatic feature engineering. This success has led to large human efforts invested into finding good network architectures. A recent alternative approach is to replace the manual design with an automated Network Architecture Search (NAS) [8]. NAS methods have succeeded in finding more complex architectures that pushed forward the state-of-the-art in both image and sequential data tasks.

One of the main drawbacks of some NAS techniques is their large computational cost. For example, the search for NASNet [43] and AmoebaNet [30], which achieve state-of-the-art results in classification [15], required 1800 and 3150 GPU days respectively. On a single GPU this corresponds to years of training time. More recent search methods, such

as ENAS [29] and DARTS [11], reduced the search time to a few GPU days, while not compromising much on accuracy. This was a major advancement, yet, there is still need for speed-up in order to make automatic search affordable and applicable to real problems.

In this paper we propose an approach that further reduces the search time to a few hours, rather than days or years. The key idea enabling this speed-up is to relax the discrete search space to be continuous, differentiable, and annealable. As noted before by DARTS [11] a continuous and differentiable search space allows for gradient-based optimization, resulting in orders of magnitude fewer computations in comparison with the black-box search, e.g., of [43, 30]. We adopt this line of thinking, but in addition we construct the search space to be annealable, i.e., emphasizing strong connections during the search in a continuous manner. We show that an annealable search space implies a more continuous optimization, and hence both faster convergence and higher accuracy.

The annealable search space we define is a key factor to both reducing the network search time and obtaining high accuracy. It allows gradual pruning of weak weights, that reduces the number of computed connections throughout the search, hence, the computational speed-up. In addition, it allows the network weights to adjust to the expected final architecture, and choose the components that are most valuable thus improving the classification accuracy of the generated architecture.

We validate the search efficiency and the performance of the generated architecture via experiments on multiple datasets. The experiments show that networks built by our algorithm achieve either higher or on par accuracy to those designed by other NAS methods, even-though our search requires only a few hours of GPU rather than days or years. Specifically, searching for 4.8 GPU-hours on CIFAR-10 produces a model that achieves a mean test error of 1.99%.

## 2. Related Work

**Architecture search techniques.** A reinforcement learning based approach has been proposed by Zoph et al. for neural architecture search [43]. They use a recurrent network as a controller to generate the model description of a child neural network designated for a given task. The resulted architecture (NASnet) improved over the existing hand-crafted network models at its time. An alternative search technique has been proposed by Real et al. [31, 30], where an evolutionary (genetic) algorithm has been used to find a neural architecture tailored for a given task. The evolved neural network [30] (AmoebaNet), improved further the performance over NASnet. Although these works achieved state-of-the-art results on various classification tasks, their main disadvantage is the amount of computational resources they demanded.

To overcome this problem, new efficient architecture search methods have been developed, showing that it is possible, with a minor loss of accuracy, to find neural architectures in just few days using only a single GPU. Two notable approaches in this direction are the differentiable architecture search (DARTS) [11] and the efficient NAS (ENAS) [29]. ENAS is similar to NASnet [43], yet its child models share weights of their shared operations from the large computational graph. During the search phase child models performance are estimated as a guiding signal to find more promising children. The weight sharing significantly reduces the search time since the child models performance are estimated with a minimal fine-tune training.

In DARTS, the entire computational graph, which includes repeating computation cells, is learned all together. At the end of the search phase, a pruning is applied on connections and their associated operations within the cells, keeping those having the highest magnitude of their related architecture weights multipliers (which represents the connections' strength). These architecture weights are learned in a continuous way during the search phase. While DARTS achieves good accuracy, our hypothesis is that the harsh pruning which occurs only once at the end of the search phase is sub-optimal and that a gradual pruning of connections can improve both the search efficiency and accuracy.

SNAS [39] suggested an alternative method for selecting the connections in the cell. SNAS approaches the search problem as sampling from a distribution of architectures, where the distribution itself is learned in a continuous way. The distribution is expressed via slack softened one-hot variables that multiply the operations and imply their associated connection. SNAS introduces a temperature parameter that steadily decrease close to zero through time, forcing the distribution towards being degenerated, thus making slack variables closer to binary, which implies which connections should be sampled and eventually chosen. Similarly to SNAS we suggest to perform an annealing pro-

cess for connections and operations selection, but differently from SNAS we wish to learn the entire computational graph all together, while gradually annealing and pruning connections.

In YOSO [40], they apply sparsity regularization over architecture weights and in the final stage they remove useless connections and isolated operations.

While both of these works [39, 40] propose an alternative to the DARTS connections selection rule, none of them managed to surpass its accuracy on CIFAR-10. In our solution we improve both the accuracy and efficiency of the DARTS searching mechanism.

**Neural networks pruning strategies.** Many pruning techniques exist for neural networks, since the networks may contain meaningful amount of operations which provides low gain [10].

The methods for weight pruning can be divided into two main approaches: pruning a network post-training and performing the pruning during the training phase.

In *post-training pruning* the weight elimination is performed only after the network is trained to learn the importance of the connections in it [22, 12, 10]. One selection criterion removes the weights based on their magnitude. The main disadvantage of post-training methods is twofold: (i) long training time, which requires a train-prune-retrain schedule; (ii) pruning of weights in a single shot might lose some dependence between some of them that become more apparent if they are removed gradually.

*Pruning-during-training* as demonstrated in [42, 1] helps to reduce the overall training time and get a sparser network. In [42], a method for gradually pruning the network has been proposed, where the number of pruned weights at each iteration depends on the final desired sparsity and a given pruning frequency. Another work suggested a compression aware method that encourages the weight matrices to be of low-rank, which helps in pruning them in a second stage [1]. Another approach sets the coefficients that are smaller than a certain threshold to zero every K steps [20]. Another pruning method uses simulated annealing[34].

## 3. Method

Our goal is to design an efficient algorithm for architecture search. We start by defining a differentiable search space that allows gradient-based optimization. A key characteristic of the search space we define is allowing for annealing of architecture weights. We then propose a gradual pruning schedule that empirically proves to allow fast convergence into networks which achieve high classification accuracy. Last, we provide theoretical analysis that places PAC bounds on the problem.

### 3.1. Differentiable Annealable Search Space

Our approach can be viewed as a generalization of DARTS [11] into an annealable search space. The key idea behind DARTS is the definition of a continuous search space that facilitates the definition of a differentiable training objective. DARTS continuous relaxation scheme leads to an efficient optimization and a fast convergence in comparison to previous solutions. On the down side, their scheme does not encourage convergence towards a reasonably sized architecture, and produces an over-parametrized network. Therefore, hard pruning is applied over the network connections in order to derive the final *child network*. As shown in [39], this introduces a *relaxation bias* that could result in a significant drop in accuracy between the parent un-pruned network and the final child network.

To overcome this limitation we define a search space that allows gradual pruning via annealing. Our search converges gradually to the final child network without requiring a hard thresholding at the end of the search.

We construct an architecture by stacking *Normal* and *Reduction* cells, similarly to DARTS and ENAS. Thus, the architecture search boils down to searching for the best Normal and Reduction cells. A cell is represented as a directed acyclic graph, consisting of an ordered sequence of nodes. Every node  $\mathbf{x}^{(i)}$  is a feature map and each directed connection  $(i, j)$  is associated with some operation  $o^{(i,j)} \in \mathcal{O}$  that transforms  $\mathbf{x}^{(j)}$  and connects it to  $\mathbf{x}^{(i)}$ . Intermediate nodes are computed based on their predecessors,

$$\mathbf{x}^{(i)} = \sum_{j < i} o^{(i,j)}(\mathbf{x}^{(j)}) \quad (1)$$

The operations  $o^{(i,j)}$  could be, for example, convolution or max-pool layers with parameters  $\omega^{(i,j)}$ . The goal of the search phase is to select the operations  $o^{(i,j)}$  which yield an overall architecture with the best performance.

In order to find the best operation to connect between two nodes, we first connect a *Mixed Operation*  $\bar{o}^{(i,j)}$  edge, defined as a weighted average of candidate operations. The mixture allows weight annealing via a temperature parameter  $T$ :

$$\bar{o}^{(i,j)}(\mathbf{x}; T) = \sum_{o \in \mathcal{O}} \Phi_o(\alpha^{(i,j)}; T) \cdot o(\mathbf{x}) \quad (2)$$

where  $\alpha_o^{(i,j)}$  is the architecture weight associated with operation  $o \in \mathcal{O}$  at edge  $(i, j)$ , and  $\Phi_o$  forms a probability distribution.

The mixture  $\Phi_o$  should be designed such that it guides the optimization to select a single operation out of the mixture in a finite time. Initially  $\Phi_o$  should be a uniform distribution, allowing consideration of all the operations. As the iterations continue the temperature is reduced and  $\Phi_o$  should converge into a degenerated distribution that selects

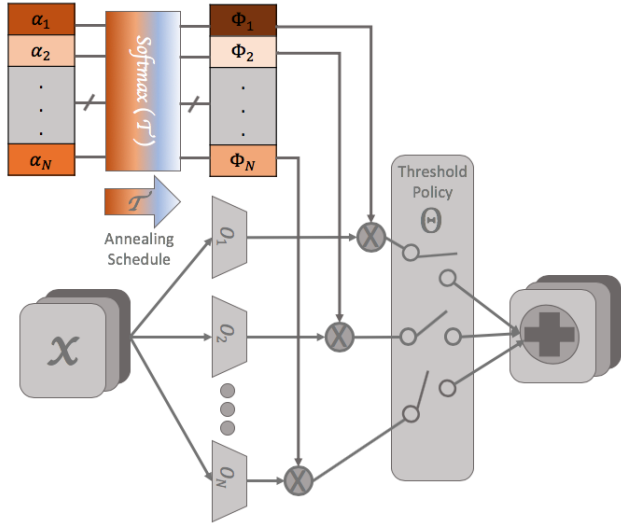


Figure 1. An illustration of our gradual annealing and pruning algorithm for architecture search depicted for a cell in the architecture. An annealing schedule is applied over architecture weights (top-left), which facilitates fast and continuous pruning of connections (right).

a single operation. Mathematically, this implies that  $\Phi_o$  should be uniform for  $T \rightarrow \infty$ , and sparse for  $T \rightarrow 0$ . We selected the following probability distribution,

$$\Phi_o(\alpha^{(i,j)}; T) = \frac{\exp\left\{\frac{\alpha_o^{(i,j)}}{T}\right\}}{\sum_{o' \in \mathcal{O}} \exp\left\{\frac{\alpha_{o'}^{(i,j)}}{T}\right\}} \quad (3)$$

This definition is closely related to the Gibbs-Boltzmann distribution, where the weights  $\alpha_o^{(i,j)}$  correspond to negative energies, and operations  $o^{(i,j)}$  to mixed system states [37]. Note, that DARTS forms a special case of our approach when setting a fixed  $T = 1$ .

### 3.2. ASAP: Architecture Search, Anneal and Prune

We are now ready to present our algorithm for Architecture Search, Anneal, and Prune (ASAP), outlined in 1 and visualized in Figure 1. ASAP anneals and prunes the connections within the cell in a continuous manner, leading to a short search time and an improved cell structure. It starts with a few “warm-up” iterations for reaching well-balanced weights. Then it optimizes over the network weights while pruning weak connections, as described next.

At initialization, all weights are randomly set. This could result in a discrepancy between parameterized operations (e.g. convolution layers) and non-parameterized operations (e.g. pooling layers). Applying pruning at this stage with imbalanced weights could lead to wrong premature decisions. Therefore, we start with performing a number of

gradient-descent based optimization steps over the network-weights only, without pruning, i.e. *grace-cycles*.

Once this warm-up ends, we perform a gradient-descent based optimization for the architecture-weights, in an alternating manner, after every network-weights optimization. Throughout this iterative process the temperature  $T$  decays according to a predefined annealing schedule. Operations are pruned if their corresponding architecture-weights go below a pruning threshold  $\theta$ , which is updated along the iterations. The annealing schedule to set  $T$  and the threshold policy governing the updates of  $\theta$  are described in section 3.3.

The process ends once we meet a stopping criterion. In our current implementation we used a simple criterion that stops when we reach a single operation per mixed operation. Other criteria could be easily adopted as well.

### 3.3. Annealing Schedule and Thresholding Policy

ASAP requires the choice of an annealing schedule  $\mathcal{T}$  determining the temperature  $T$  through time, and a threshold policy  $\Theta$  governing the updates of the pruning threshold  $\theta$ . This choice is dominated by a trade-off. On one hand, pruning-during-training simplifies the optimization objective and reduces the complexity, assisting the network to converge and reducing overfitting. In addition, it accelerates the search process, since pruned operations are removed from the optimization. This implies the choice of fast temperature decay and a harsh thresholding. However, on the other hand, premature pruning of operations during the search could lead to a sub-optimal child network. This suggests we should choose a slow temperature decay and a soft thresholding.

To choose schedule and policy that balance this trade-off we present in Section 3.4 theoretical analysis and functional forms for  $(\mathcal{T}, \Theta)$  that guarantee under some assumptions that Algorithm 1 is  $(0, \delta)$ -PAC, i.e. it selects the best operation with probability  $1 - \delta$ , see Definition 1. In other words, we show that with a proper annealing and thresholding the algorithm has a high likelihood to prune only sub-optimal operations. However, while these theoretical results are strong, the critical schedule they suggest is rather slow, because PAC bounds tend to be overly pessimistic in practice. Therefore, for practical usage we suggest a more aggressive schedule.

The solution we propose is based on observations explored in Simulated Annealing, which shares a similar trade-off between the continuity of the optimization process and the time required for deriving the solution [2]. Among the many alternatives we choose the exponential schedule, which has been shown to be effective when the optimization steps are expensive, e.g. [16],[28],[19],

$$\mathcal{T}(t) = T_0 \beta^t \quad (4)$$

This schedule starts with a relatively high temperature  $T_0$  and decays fast. As for the pruning threshold, we chose the simplest solution of a fixed value  $\Theta \equiv \theta_0$ . We demonstrate the effectiveness of our choices via experiments in Section 4.

---

#### Algorithm 1 ASAP for a single Mixed Operation

---

- 1: **Input:** Operations  $o_i \in \mathcal{O} \quad i \in \{1, \dots, N\}$ ,  
Annealing schedule  $\mathcal{T}$ ,  
Grace-temperature  $\tau$ ,  
Threshold policy  $\Theta$ ,
  - 2: **Init:**  $T \leftarrow \mathcal{T}(0), \theta \leftarrow \Theta(0) \quad \alpha_i \leftarrow 0 \quad i \in \{1, \dots, N\}$ .
  - 3: **while**  $|\mathcal{O}| > 1$  **do**
  - 4:   Update  $\omega$  by descend step over  $\nabla_{\omega} \mathcal{L}_{\text{train}}(\omega, \alpha; T)$
  - 5:   **if**  $T < \tau$  **then**
  - 6:     Update  $\alpha$  by descend step over  $\nabla_{\alpha} \mathcal{L}_{\text{val}}(\omega, \alpha; T)$
  - 7:     **for each**  $o_i \in \mathcal{O}$  such that  $\Phi_{o_i}(\alpha; T) < \theta$  **do**
  - 8:        $\mathcal{O} = \mathcal{O} \setminus \{o_i\}$
  - 9:     **end for**
  - 10:   **end if**
  - 11:   Update  $T$  according to  $\mathcal{T}$
  - 12:   Update  $\theta$  according to  $\Theta$
  - 13: **end while**
  - 14: **return**  $\mathcal{O}$
- 

### 3.4. Theoretical Analysis

The pruning we are dealing with can be viewed as a selection problem, i.e., pruning all the inferior operations, such that the one with the highest expected architecture weight remains, while only the empirical value is measured. We prove PAC bounds for the underlying selection problem.

**Definition 1** ( $(0, \delta)$ -PAC) *An algorithm that outputs the best operation with probability  $1 - \delta$  is  $(0, \delta)$ -PAC.*

**Theorem 2** *Assuming  $\nabla_{\alpha_{t,i}} \mathcal{L}_{\text{val}}(\omega, \alpha; T_t)$  is independent through time and bounded by  $\mathbf{L}$  in absolute value for all  $t$  and  $i$ , then Algorithm 1 with a threshold policy,*

$$\theta_t = \nu_t e^{-t} \quad (5)$$

$$\nu_t \in \Upsilon = \left\{ \nu_t \mid \nu_t \geq 0; \lim_{t \rightarrow \infty} \frac{\log(\nu_t)}{t} = 0 \right\} \quad (6)$$

and an annealing schedule,

$$\mathcal{T}(t) = \eta \mathbf{L} \rho_t \sqrt{\frac{8}{t} \log \left( \frac{\pi^2 N t^2}{3\delta} \right)} \quad (7)$$

$$\rho_t = \frac{t}{t + \log \left( \frac{1}{N \nu_t} \right)} \quad (8)$$

is  $(0, \delta)$ -PAC.

The proof of the theorem relies on two main steps: (i) Reducing the algorithm to a *Successive-Elimination* method [9], and (ii) Bounding the probability of deviation of  $\alpha$  from its expected value. We sketch the proof using Claim 1 and Theorem 3 below.

**Claim 1** *The pruning rule (Step 7) in Algorithm 1 is equivalent to pruning  $o_i \in \mathcal{O}$  at time  $t$  if,*

$$\frac{\alpha_{t,i}}{t} + \beta_t < \frac{\alpha_t^*}{t} - \beta_t, \quad (9)$$

where  $\alpha_t^* = \max_i \{\alpha_{t,i}\}$  and  $\beta_t = \frac{T_t}{2\rho_t}$ .

Although involving the empirical values of  $\alpha$ , the condition in Claim 1 avoids the pruning of the operation with the highest expected  $\alpha$ . For this purpose we bound the probability for the deviation of each empirical  $\alpha$  from its expected value by the specified margin  $\beta_t$ . We provide Theorem 3, which states that for any time  $t$  and operation  $o_i \in \mathcal{O}$ , the value of  $\frac{\alpha_{t,i}}{t}$  is within  $\beta_t$  of its expected value  $\frac{\bar{\alpha}_{t,i}}{t} = \frac{1}{t} \sum_{s=1}^t \mathbb{E}[g_{s,i}]$ , where,

$$g_{t,i} = -\eta \nabla_{\alpha_{t,i}} \mathcal{L}_{val}(w, \alpha; T_t) \in [-\eta \mathbf{L}, \eta \mathbf{L}]. \quad (10)$$

**Theorem 3** *For any time  $t$  and operation  $\{o_i\}_{i=1}^N \in \mathcal{O}$ , we have,*

$$\mathbb{P} \left\{ \frac{1}{t} |\alpha_{t,i} - \bar{\alpha}_{t,i}| \leq \beta_t \right\} \geq 1 - \frac{\delta}{N}. \quad (11)$$

Requiring this to hold for all the  $N$  operations, we get that the probability of pruning the best operation is below  $1 - \delta$ . Choosing an annealing schedule and threshold policy such that  $\beta_t$  goes to zero as  $t$  increases, guarantees that eventually all operations but the best one are pruned. This leads to the desired result. Full proofs appear in the supplementary material.

## 4. Experiments

To show the effectiveness of ASAP we test it on common benchmarks and compare to the state-of-the-art. We experimented on the very popular benchmarks, CIFAR-10 and ImageNet, as well as on five other classification datasets, for providing a more extensive evaluation. In addition, we explore alternative pruning methods and compare ASAP to them.

### 4.1. Architecture Search on CIFAR-10

We search on CIFAR-10 for convolutional cells in a small parent network. Then we build a larger network by stacking the learned cells, train it on CIFAR-10 and compare the results against some common NAS methods.

We create a parent network by stacking eight cells with architecture weights sharing. Each cell contains four ordered nodes, each of which is connected via mixed operations to all previous nodes in the cell and also to the two previous cells' outputs. Each mixed operation contains seven operations: 3x3 and 5x5 separable and dilated separable convolutions, 3x3 max-pooling, 3x3 average-pooling and an identity. The output of a cell is a concatenation of the outputs of all the nodes within the cell.

The search phase lasts until each mixed operation is fully pruned, or until we reach 50 epochs. We use the first-order approximation [11], relating to  $\alpha$  and  $\omega$  as independent thus can be optimized separately. The train set is divided into two parts of equal sizes: one is used for training the operations' weights  $\omega$  and the other for training the architecture weights  $\alpha$ .

For the gradual annealing and pruning process, we use an initial temperature of  $T_0 = 1.3$  and an epoch decay factor of  $\beta = 0.95$ , thus  $T \approx 0.1$  at the end of the search phase. Considering we have  $N$  possible operations to choose from in a mixed operation, we set our pruning threshold to  $\theta_t \equiv \frac{0.4}{N}$ . Other hyper-parameters follow [11].

As the search progresses, continuous pruning reduces the network size. With a batch size of 96, one epoch takes 5.8 minutes in average on a single GPU<sup>1</sup>, summing up to 4.8 hours in total for a single search.

Figure 2 illustrates an example of the epoch duration and the network sparsity (1 minus the relative part of the pruned connections) during a search. The smooth removal of connections is evident. This translates to a significant decrease in an epoch duration along the search. Note that the first five epochs are grace-cycles, where only the network weights are trained as no operations are pruned.

Figures 3 and 4 show our learned normal and reduction cells, respectively.

### 4.2. CIFAR-10 Evaluation Results

We build a network by stacking 20 cells and 36 initial channels, train it from scratch for 600 epochs using a batch size of 96. Following [11], we use a cosine annealing learning rate [25], cutout [7], drop-path [21] and auxiliary towers [35] as well as random horizontal flipping and cropping augmentations. A full training takes 1 GPU day (2.5 minutes per epoch), hence the duration of an end-to-end search and train on CIFAR-10 is 1.25 GPU days. In addition, we define an enhanced training (ET) variant, where a larger network, with 44 initial channels, is trained for 1200 epochs with AutoAugment [4]. Table 1 shows the performance of our learned models compared to other state-of-the-art NAS methods. Figure 5 provides an even more comprehensive comparison in a graphical manner.

<sup>1</sup>Experiments were performed using a NVIDIA GTX 1080Ti GPU.

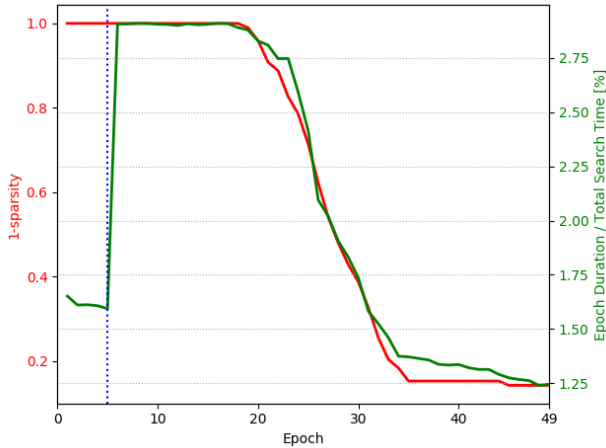


Figure 2. Relative epoch duration during search and model 1-sparsity vs epoch number. The dotted line represents grace cycles.

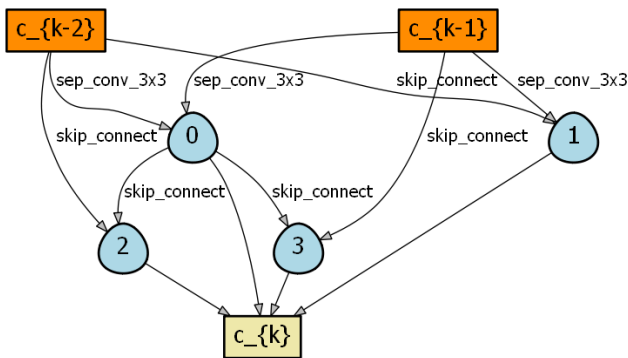


Figure 3. ASAP learned normal cell on CIFAR-10.

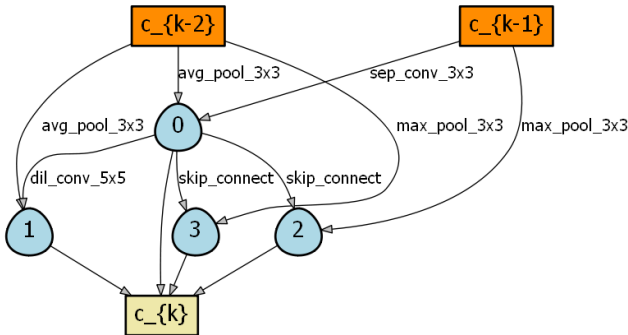


Figure 4. ASAP learned reduction cell on CIFAR-10.

Table 1 and Figure 5 show that without bells and whistles, our ASAP based network outperforms previous state-of-the-art methods, both in terms of the classification error

Architecture	Test error (%)	Params (M)	Search cost
AmoebaNet-A [30]	$3.34 \pm 0.06$	3.2	3150
AmoebaNet-B [30]	$2.55 \pm 0.05$	2.8	3150
NASNet-A [44]	2.65	3.3	1800
PNAS [24]	3.41	3.2	150
SNAS [39]	$2.85 \pm 0.02$	2.8	1.5
DSO-NAS [40]	$2.95 \pm 0.12$	3	1
PARSEC [3]	$2.81 \pm 0.03$	3.7	1
DARTS(2nd) [11]	$2.76 \pm 0.06$	3.4	1
ENAS [29]	2.89	4.6	0.5
DARTS(1nd) [11]	2.94	2.9	0.4
NAONet-WS [26]	3.53	<b>2.5</b>	0.3
ASAP	$2.49 \pm 0.04$	<b>2.5</b>	<b>0.2</b>
ASAP + ET	<b><math>1.99 \pm 0.05</math></b>	3.7	<b>0.2</b>

Table 1. Classification errors of ASAP compared to state-of-the-art NAS methods on CIFAR-10. The Search cost is measured in GPU days.

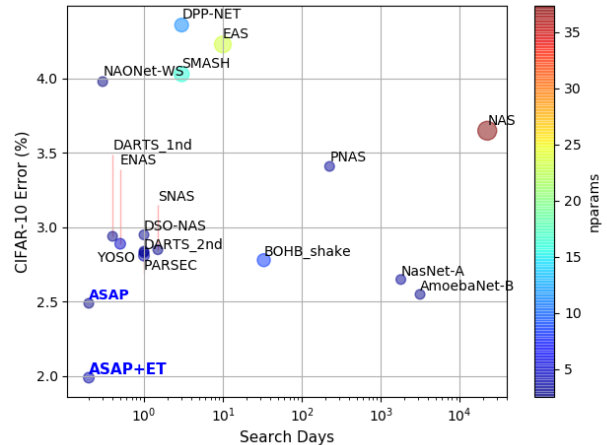


Figure 5. Comparison of CIFAR-10 error vs search days of top NAS methods. Marker size is correlated with the memory footprint.

and the search time, while having the smallest number of parameters.

Note that NasNet, AmoebaNet and some other cells have variants, e.g. [44], [15], of much larger networks that achieve improved results on CIFAR-10. For the sake of reasonable comparison, in Table 1 we restrict ourselves to architectures with up to 10M parameters.

### 4.3. Transferability Evaluation

**ImageNet** For testing the performance on larger datasets, we experiment on the popular ImageNet dataset [6]. Our cell, found through searching on CIFAR-10, is trained on ImageNet for examining the cell transferability to larger datasets. The network is composed of 14 stacked

cells with two initial stem cells. We train the network for 250 epochs, following the training scheme and hyper-parameters given in [11]. The results are presented in Table 2. It can be seen that the network found by ASAP transfers well to ImageNet, achieving a competitive accuracy compared to other top methods, with a significantly faster search.

**Other classification datasets** We further extend the transferability evaluation by training our ASAP cell and other top published NAS cells on several common computer vision classification datasets:

**CINIC-10:** [5] is an extension of CIFAR-10 by ImageNet images, down-sampled to match the image size of CIFAR-10. It has 270,000 images of 10 classes, i.e. it has larger train and test sets than those of CIFAR-10.

**CIFAR-100:** [36] A natural image classification dataset, containing 100 classes with 600 images per class. The image size is 32x32 and the train-test split is 50,000:10,000 images respectively.

**FREIBURG:** [17] A groceries classification dataset consisting of 5000 images of size 256x256, divided into 25 categories. It has imbalanced class sizes ranging from 97 to 370 images per class. Images were taken in various aspect ratios and padded to squares.

**SVHN:** [27] A dataset containing real-world images of digits and numbers in natural scenes. It consists of 600,000 images of size 32x32, divided into 10 classes. The dataset can be thought of as a real-world alternative to MNIST, with an order of magnitude more images and significantly harder real-world scenarios.

**FMNIST:** [38] A clothes classification dataset with a 60,000:10,000 train-test split. Each example is a grayscale image of size 28x28, associated with a label from 10 classes of clothes. It is intended to serve as a direct drop-in replacement for the original MNIST dataset as a benchmark for machine learning algorithms.

For a fair comparison, presented in Table 2, we train all of the cells using the publicly available DARTS training code <sup>2</sup>, with exactly the same network configuration and hyper-parameters, except from the cell itself.

Table 2 shows that our ASAP cell transfers well to other computer vision datasets, surpassing all other NAS cells in four out of five of the datasets tested. In addition, note that on two datasets, CINIC-10 and FREIBURG, our ASAP network accuracy is better than the previously known state-of-the-art. Together with the low computational search cost of ASAP, the success of the proposed method is demonstrated.

#### 4.4. Other Pruning Methods

In addition to comparisons to other SotA algorithms, we also evaluate alternative pruning-during-training techniques. We select two well known pruning approaches and

<sup>2</sup><https://github.com/quark0/darts>

adapt those to the neural architecture search framework. The first approach is magnitude based. It naively cuts connections with the smallest weights, as is the practice in some network pruning strategies, e.g. [10, 42] (as well as in [11], yet with a harsh single pruning-after-training step). The second approach [23] prunes connections with the lowest accumulated absolute value of the gradients of the loss with respect to  $\alpha$ .

Our evaluation is based on the number of operations to prune in each step, according to the formula suggested in [42]:

$$s_t = s_f + (s_i - s_f) \left(1 - \frac{t - t_0}{n\Delta t}\right)^p \quad (12)$$

where  $p \in \{1, 3\}$ ,  $t \in \{t_0, t_0 + \Delta t, \dots, t_0 + n\Delta t\}$ ,  $s_f$  is the final desired sparsity (the fraction of pruned weights),  $s_i$  is the initial sparsity, which is 0 in our case,  $t_0$  is the iteration we start the pruning at, and  $E_f = t_0 + n\Delta t$  is the total number of iterations used for the search. For  $p = 1$  the pruning rate is constant, while for  $p = 3$  it decreases. The evaluation was performed on CIFAR-10 with  $t_0 = 20$  and  $E_f$  in the range from 50 to 70.

Table 3 presents the results. Both pruning methods achieved lower accuracy than ASAP on CIFAR-10, with larger memory footprint.

#### 4.5. Search Process Analysis

In this section we wish to provide further insights as to why ASAP leads to a higher accuracy for a lower search time. To do that we explore two properties along the iterative learning process: the validation accuracy and the cell entropy. We compare ASAP to two other efficient methods: DARTS [11], and the reinforcement-learning based ENAS [29]. We further compare to the pruning alternative based on accumulated gradients described in Section 4.4, as it achieved better results on CIFAR-10 as shown in Table 3. We compare with both  $p \in \{1, 3\}$ .

Figure 6 presents the validation accuracy along the architecture search iterations. ENAS achieves low and noisy accuracy along the search, inferior to all differentiable-space based methods. DARTS accuracy climbs nicely across iterations, but then significantly drops at the end of the search due to the relaxation bias following the harsh prune. The pruning-during-training methods suffer from perturbations in accuracy following pruning, however, ASAP’s perturbations are frequent and smaller, as its architecture-weights which get pruned are insignificant. Its validation accuracy quickly recovers due to the continuous annealing of weights. Therefore, With reduced network complexity, it achieves the highest accuracy at the end.

Figure 7 illustrates the average cell entropy over time, averaged across all the mixed operations within the cell, normalized by  $\ln(|\mathcal{O}|)$ . While the entropy of DARTS and

Architecture	CINIC-10 Error(%)	FREIBURG Error(%)	CIFAR-100 Error(%)	SVHN Error(%)	FMNIST Error(%)	ImageNet Error(%)	Search cost
Known SotA	8.6 [5]	21.1 [17]	8.7 [15]	1.02 [4]	3.65 [41]	15.7 [15]	-
AmoebaNet-A [30]	7.18	11.8	15.9	1.93	3.8	<b>24.3</b>	3150
NASNet [44]	6.93	13.4	15.8	1.96	3.71	26.0	1800
PNAS [24]	7.03	12.3	15.9	1.83	3.72	25.8	150
SNAS [39]	7.13	14.7	16.5	1.98	3.73	27.3	1.5
DARTS-Rev1 [11]	7.05	11.4	15.8	1.94	3.74	26.9	1
DARTS-Rev2 [11]	6.88	10.8	15.7	1.85	<b>3.68</b>	26.7	1
ASAP	<b>6.83</b>	<b>10.7</b>	<b>15.6</b>	<b>1.81</b>	3.73	26.7	<b>0.2</b>

Table 2. The classification error of ASAP, compared to top NAS cells, on several vision classification datasets. Error refers to top-1 test error. Search cost is measured in GPU days. DARTS Rev1 and Rev2 refers to the best 2nd order cells published in revision 1 and 2 of [11] respectively.

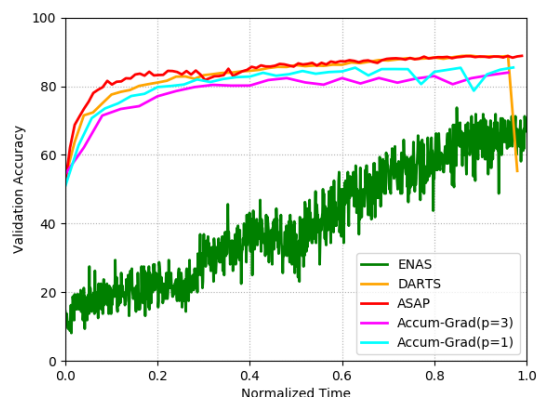


Figure 6. The validation accuracy during search for ENAS, DARTS, ASAP and Accum-Grad vs the time (scaled to [0, 1]).

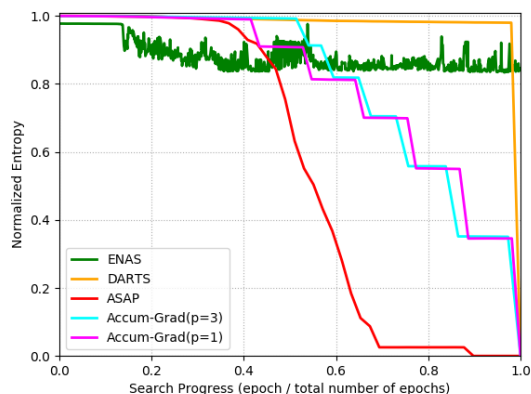


Figure 7. The total normalized entropy during search of normal and reduction cells together for ENAS and for the normal cell alone for DARTS, ASAP and Accum-Grad vs the time scaled to [0, 1].

Architecture type	Test error Top-1(%)	Params (M)
DARTS(2st)	$2.76 \pm 0.06$	3.4
Magnitude prune	$3.05 \pm 0.15$	4.4
Accum-Grad prune	$2.86 \pm 0.1$	4.3
ASAP	$2.49 \pm 0.04$	2.5

Table 3. Comparison of pruning methods on CIFAR-10.

ENAS remain high along the entire search, the entropy of the pruning methods decrease to zero as those do not suffer from a relaxation bias. The high entropy of DARTS when final prune is done leads to a quite arbitrary selection of a child model, as top architecture weights are of comparable value. It can be seen that the entropy of ASAP decreases gradually, hence allowing efficient optimization in the differentiable-annealable space. This provides further motivation to the advantages of ASAP.

## 5. Conclusion

In this paper we presented ASAP, an efficient state-of-the-art neural architecture search framework. The key contribution of ASAP is the annealing and gradual pruning of connections during the search process. This approach avoids hard pruning of connections that is used by other methods. The gradual pruning decreases the architecture search time, while improving the final accuracy due to smoother removal of connections during the search phase.

On CIFAR-10, our ASAP cell outperforms other published cells, both in terms of search cost and in terms of test error. We also demonstrate the effectiveness of ASAP cell by showing superior transferability quality compared to other top NAS cells on multiple computer vision datasets.

We believe that our approach to gradual annealing and pruning can lead the way to even more efficient and effective search methods also for full architecture search.

## References

- [1] J. M. Alvarez and M. Salzmann. Compression-aware training of deep networks. In *Advances in Neural Information Processing Systems (NIPS)*, 2017. **2**
- [2] F. Busetti. Simulated annealing overview. *World Wide Web URL www.geocities.com/francorbusetti/saweb.pdf*, 2003. **4**
- [3] F. P. Casale, J. Gordon, and N. Fusi. Probabilistic neural architecture search. *arXiv preprint arXiv:1902.05116*, 2019. **6**
- [4] E. D. Cubuk, B. Zoph, D. Mane, V. Vasudevan, and Q. V. Le. Autoaugment: Learning augmentation policies from data. *arXiv preprint arXiv:1805.09501v2*, 2018. **5, 8, 13**
- [5] L. N. Darlow, E. J. Crowley, A. Antoniou, and A. J. Storkey. Cinic-10 is not imagenet or cifar-10. *arXiv preprint arXiv:1810.03505*, 2018. **7, 8, 13**
- [6] J. Deng, W. Dong, R. Socher, L.-J. Li, K. Li, and L. Fei-Fei. ImageNet: A Large-Scale Hierarchical Image Database. In *CVPR09*, 2009. **6**
- [7] T. DeVries and G. W. Taylor. Improved regularization of convolutional neural networks with cutout. *arXiv preprint arXiv:1708.04552*, 2017. **5, 12**
- [8] T. Elsken, J. H. Metzen, and F. Hutter. Neural architecture search: A survey. *arXiv preprint arXiv:1808.05377*, 2018. **1**
- [9] E. Even-Dar, S. Mannor, and Y. Mansour. Action elimination and stopping conditions for the multi-armed bandit and reinforcement learning problems. *Journal of machine learning research*, 7(Jun):1079–1105, 2006. **5**
- [10] S. Han, J. Pool, J. Tran, and W. J. Dally. Learning both weights and connections for efficient neural networks. In *Advances in Neural Information Processing Systems (NIPS)*, 2015. **2, 7**
- [11] L. Hanxiao, S. Karen, and Y. Yiming. Darts: Differentiable architecture search. In *International Conference on Learning Representations (ICLR)*, 2019. **1, 2, 3, 5, 6, 7, 8, 12**
- [12] B. Hassibi and D. G. Stork. Second order derivatives for network pruning: Optimal brain surgeon. In *Advances in Neural Information Processing Systems (NIPS)*, 1993. **2**
- [13] W. Hoeffding. Probability inequalities for sums of bounded random variables. *Journal of the American Statistical Association*, 58(301):13–30, 1963. **11**
- [14] A. G. Howard, M. Zhu, B. Chen, D. Kalenichenko, W. Wang, T. Weyand, M. Andreetto, and H. Adam. Mobilenets: Efficient convolutional neural networks for mobile vision applications. *arXiv preprint arXiv:1704.04861*, 2017. **12**
- [15] Y. Huang, Y. Cheng, D. Chen, H. Lee, J. Ngiam, Q. V. Le, and Z. Chen. Gpipe: Efficient training of giant neural networks using pipeline parallelism. *arXiv preprint arXiv:1811.06965*, 2018. **1, 6, 8**
- [16] L. Ingber. Very fast simulated re-annealing. *Mathematical and computer modelling*, 12(8):967–973, 1989. **4**
- [17] P. Jund, N. Abdo, A. Eitel, and W. Burgard. The freiburg groceries dataset. *arXiv preprint arXiv:1611.05799*, 2016. **7, 8, 13**
- [18] D. P. Kingma and J. Ba. Adam: A method for stochastic optimization. *arXiv preprint arXiv:1412.6980*, 2014. **12**
- [19] S. Kirkpatrick, C. D. Gelatt, and M. P. Vecchi. Optimization by simulated annealing. *science*, 220(4598):671–680, 1983. **4**
- [20] J. Langford, L. Li, and T. Zhang. Sparse online learning via truncated gradient. In *Journal of Machine Learning Research*, 2008. **2**
- [21] G. Larsson, M. Maire, and G. Shakhnarovich. Fractalnet: Ultra-deep neural networks without residuals. *arXiv preprint arXiv:1605.07648*, 2016. **5, 12**
- [22] Y. LeCun, J. S. Denker, and S. A. Solla. Optimal brain damage. In *Advances in Neural Information Processing Systems (NIPS)*, 1990. **2**
- [23] M. G. G. L. M. Lis. Dropback: Continuous pruning during training. *arXiv preprint arXiv:1806.06949*, 2018. **7**
- [24] C. Liu, B. Zoph, M. Neumann, J. Shlens, W. Hua, L.-J. Li, L. Fei-Fei, A. Yuille, J. Huang, and K. Murphy. Progressive neural architecture search. In *Proceedings of the European Conference on Computer Vision (ECCV)*, pages 19–34, 2018. **6, 8**
- [25] I. Loshchilov and F. Hutter. Sgdr: Stochastic gradient descent with warm restarts. *arXiv preprint arXiv:1608.03983*, 2016. **5, 12**
- [26] R. Luo, F. Tian, T. Qin, E. Chen, and T.-Y. Liu. Neural architecture optimization. In *Advances in Neural Information Processing Systems*, pages 7827–7838, 2018. **6**
- [27] Y. Netzer, T. Wang, A. Coates, A. Bissacco, B. Wu, and A. Y. Ng. Reading digits in natural images with unsupervised feature learning. 2011. **7, 13**
- [28] Y. Nourani and B. Andresen. A comparison of simulated annealing cooling strategies. *Journal of Physics A: Mathematical and General*, 31(41):8373, 1998. **4**
- [29] H. Pham, M. Y. Guan, B. Zoph, Q. V. Le, and J. Dean. Efficient neural architecture search via parameter sharing. In *International Conference on Machine Learning (ICML)*, 2018. **1, 2, 6, 7**
- [30] E. Real, A. Aggarwal, Y. Huang, and Q. V. Le. Regularized evolution for image classifier architecture search. In *International Conference on Machine Learning - ICML AutoML Workshop*, 2018. **1, 2, 6, 8, 12**
- [31] E. Real, S. Moore, A. Selle, S. Saxena, Y. L. Suematsu, J. Tan, Q. V. Le, and A. Kurakin. Large-scale evolution of image classifiers. In *International Conference on Machine Learning (ICML)*, 2017. **2**
- [32] S. Reed, H. Lee, D. Anguelov, C. Szegedy, D. Erhan, and A. Rabinovich. Training deep neural networks on noisy labels with bootstrapping. *arXiv preprint arXiv:1412.6596*, 2014. **12**
- [33] H. Robbins and S. Monro. A stochastic approximation method. *The annals of mathematical statistics*, pages 400–407, 1951. **12**
- [34] S. W. Stepniewski and A. J. Keane. Pruning backpropagation neural networks using modern stochastic optimisation techniques. In *Neural Computing and Applications*, 1997. **2**
- [35] C. Szegedy, W. Liu, Y. Jia, P. Sermanet, S. Reed, D. Anguelov, D. Erhan, V. Vanhoucke, and A. Rabinovich. Going deeper with convolutions. In *Proceedings of the IEEE conference on computer vision and pattern recognition*, pages 1–9, 2015. **5, 12**

- [36] A. Torralba, R. Fergus, and W. T. Freeman. 80 million tiny images: A large data set for nonparametric object and scene recognition. *IEEE transactions on pattern analysis and machine intelligence*, 30(11):1958–1970, 2008. 7, 13
- [37] P.J. Van Laarhoven and E. H. Aarts. Simulated annealing. In *Simulated annealing: Theory and applications*, pages 7–15. Springer, 1987. 3
- [38] H. Xiao, K. Rasul, and R. Vollgraf. Fashion-mnist: a novel image dataset for benchmarking machine learning algorithms. *arXiv preprint arXiv:1708.07747*, 2017. 7, 13
- [39] S. Xie, H. Zheng, C. Liu, and L. Lin. Snas: Stochastic neural architecture search. In *International Conference on Learning Representations (ICLR)*, 2019. 2, 3, 6, 8
- [40] X. Zhang, Z. Huang, and N. Wang. You only search once: Single shot neural architecture search via direct sparse optimization. *arxiv 1811.01567*, 2018. 2, 6
- [41] Z. Zhong, L. Zheng, G. Kang, S. Li, and Y. Yang. Random erasing data augmentation. *arXiv preprint arXiv:1708.04896*, 2017. 8
- [42] M. Zhu and S. Gupta. To prune, or not to prune: exploring the efficacy of pruning for model compression. In *2017 NIPS Workshop on Machine Learning of Phones and other Consumer Devices*, 2017. 2, 7
- [43] B. Zoph and Q. V. Le. Neural architecture search with reinforcement learning. In *International Conference on Learning Representations (ICLR)*, 2017. 1, 2, 12
- [44] B. Zoph, V. Vasudevan, J. Shlens, and Q. V. Le. Learning transferable architectures for scalable image recognition. In *Proceedings of the IEEE conference on computer vision and pattern recognition*, pages 8697–8710, 2018. 6, 8

## 6. Supplementary Material

### 6.1. Proof of Theorem 2

Let us set some terms,

$$g_{t,i} = -\eta \nabla_{\alpha_{t,i}} \mathcal{L}_{val}(w, \alpha; T_t) \quad (13)$$

Then we have  $|g_{t,i}| \leq \eta \cdot \mathbf{L}$  and,

$$\alpha_{t,i} = \alpha_{0,i} - \eta \sum_{s=0}^t \nabla_{\alpha_{s,i}} \mathcal{L}_{val}(w, \alpha; T_t) = \sum_{s=0}^t g_{s,i} \quad (14)$$

As we initialize  $\alpha_{0,i} = 0$  for all  $i = 1, \dots, N$  in 2.

Then we prove claim 1,

**Proof:** The pruning rule can be put as following,

$$\Phi_{o_i}(\alpha_t; T_t) < \theta_t \quad (15)$$

$$\frac{e^{\frac{\alpha_{t,i}}{T_t}}}{\sum_{j=1}^N e^{\frac{\alpha_{t,i}}{T_t}}} < \theta_t \quad (16)$$

$$\alpha_{t,i} < T_t \log \left( \sum_{j=1}^N e^{\frac{\alpha_{t,i}}{T_t}} \right) - T_t \log \left( \frac{1}{\theta_t} \right) \quad (17)$$

$$\leq T_t \left( \frac{\alpha_t^*}{T_t} + \log(N) \right) - T_t \log \left( \frac{1}{\theta_t} \right) \quad (18)$$

$$< \alpha_t^* - T_t \left( \log \left( \frac{1}{\theta_t} \right) - \log(N) \right) \quad (19)$$

$$< \alpha_t^* - T_t \left( t + \log \left( \frac{1}{N\nu_t} \right) \right) \quad (20)$$

$$< \alpha_t^* - tT_t\rho_t^{-1} \quad (21)$$

$$< \alpha_t^* - 2t\beta_t \quad (22)$$

Where 20 is by setting  $\theta_t = \nu_t e^{-t}$  and 18 is since,

$$\log \left( \sum_{i=1}^N e^{x_i} \right) \leq \max_i x_i + \log(N) \quad (23)$$

Finally we have,

$$\frac{\alpha_{t,i}}{t} + \beta_t < \frac{\alpha_t^*}{t} - \beta_t, \quad (24)$$

We wish to bound the probability of pruning the best operation, i.e. the operation with the highest expected architecture parameter  $\alpha$ . Although involving the empirical values of  $\alpha$ , we show that the condition in claim 1 avoids the pruning of the operation with the highest expected  $\alpha$ . For this purpose we bound the probability for the deviation of each empirical  $\alpha$  from its expected value by the specified margin  $\beta_t$ . For this purpose we introduce the following concentration bound,

**Lemma 1 (Hoeffding [13])** Let  $g_1, \dots, g_t$  be independent bounded random variables with  $g_s \in [a_s, b_s]$ , where  $-\infty < a_s \leq b_s < \infty$  for all  $s = 1, \dots, t$ . Then,

$$\mathbb{P} \left\{ \frac{1}{t} \sum_{s=1}^t (g_s - \mathbb{E}[g_s]) \geq \beta \right\} \leq e^{-\frac{2\beta^2 t^2}{\sum_{s=1}^t (b_s - a_s)^2}} \quad (25)$$

$$\mathbb{P} \left\{ \frac{1}{t} \sum_{s=1}^t (g_s - \mathbb{E}[g_s]) \leq -\beta \right\} \leq e^{-\frac{2\beta^2 t^2}{\sum_{s=1}^t (b_s - a_s)^2}} \quad (26)$$

Our main argument, described in Theorem 3, is that at any time  $t$  and for any operation  $o_i$ , the empirical value  $\frac{\alpha_{t,i}}{t}$  is within  $\beta_t$  of its expected value  $\frac{\bar{\alpha}_{t,i}}{t} = \frac{1}{t} \sum_{s=1}^t \mathbb{E}[g_{s,i}]$ . For the purpose of proving Theorem 3, we first prove the following Corollary 4,

**Corollary 4** For any time  $t$  and operations  $\{o_i\}_{i=1}^N \in \mathcal{O}$  we have,

$$\mathbb{P} \left\{ \frac{1}{t} |\alpha_{t,i} - \bar{\alpha}_{t,i}| > \beta_t \right\} \leq \frac{6\delta}{\pi^2 N t^2} \quad (27)$$

**Proof:**

$$\mathbb{P} \left\{ \frac{1}{t} |\alpha_{t,i} - \bar{\alpha}_{t,i}| > \beta_t \right\} \quad (28)$$

$$= \mathbb{P} \left\{ \frac{\alpha_{t,i}}{t} - \frac{\bar{\alpha}_{t,i}}{t} > \beta_t \cup \frac{\alpha_{t,i}}{t} - \frac{\bar{\alpha}_{t,i}}{t} < -\beta_t \right\} \quad (29)$$

$$\leq \mathbb{P} \left\{ \frac{\alpha_{t,i}}{t} - \frac{\bar{\alpha}_{t,i}}{t} > \beta_t \right\} + \mathbb{P} \left\{ \frac{\alpha_{t,i}}{t} - \frac{\bar{\alpha}_{t,i}}{t} < -\beta_t \right\} \quad (30)$$

$$\leq \mathbb{P} \left\{ \frac{1}{t} \sum_{s=1}^t (g_{s,i} - \mathbb{E}[g_{s,i}]) \geq \beta_t \right\} + \mathbb{P} \left\{ \frac{1}{t} \sum_{s=1}^t (g_{s,i} - \mathbb{E}[g_{s,i}]) \leq -\beta_t \right\} \quad (31)$$

$$\leq 2e^{-\frac{2\beta_t^2 t}{4\eta^2 \mathbf{L}^2}} \quad (32)$$

$$\leq \frac{6\delta}{\pi^2 N t^2} \quad (33)$$

Where, 30 is by the union bound, 32 is by Lemma 1 with  $g_{t,i} \in [-\eta \mathbf{L}, \eta \mathbf{L}]$  and 33 is by setting,

$$\beta_t = \eta \mathbf{L} \sqrt{\frac{2}{t} \log \left( \frac{\pi^2 N t^2}{3\delta} \right)} \quad (34)$$

We can now prove Theorem 3,

**Proof:**

$$\mathbb{P} \left\{ \bigcap_{t=1}^{\infty} \frac{1}{t} |\alpha_{t,i} - \bar{\alpha}_{t,i}| \leq \beta_t \right\} \quad (35)$$

$$= 1 - \mathbb{P} \left\{ \bigcup_{t=1}^{\infty} \frac{1}{t} |\alpha_{t,i} - \bar{\alpha}_{t,i}| > \beta_t \right\} \quad (36)$$

$$\geq 1 - \sum_{t=1}^{\infty} \mathbb{P} \left\{ \frac{1}{t} |\alpha_{t,i} - \bar{\alpha}_{t,i}| > \beta_t \right\} \quad (37)$$

$$\geq 1 - \frac{6\delta}{\pi^2 N} \sum_{t=1}^{\infty} \frac{1}{t^2} \quad (38)$$

$$= 1 - \frac{\delta}{N} \quad (39)$$

where (37) is by the union bound, (38) is by Corollary 4.

Requiring Theorem 3 to hold for all of the operations, we get by the union bound that, the probability of pruning the best operation is less than  $\delta$ . Furthermore, since  $\nu_t \in \Upsilon$ ,  $\rho_t$  goes to 1 as  $t$  increases and  $T_t$  goes to zero together with  $\beta_t$ . Thus eventually all operations but the best one are pruned. This completes our proof.

## 6.2. ASAP search and train details

In order to conduct a fair comparison, we follow [11] for all the search and train details. This excludes the new annealing parameters and those related to the training of additional datasets, which are not mentioned in [11]. Our code will be made available for future public use.

### 6.2.1 Search details

**Data pre-processing.** We apply the following:

- Centrally padding the training images to a size of 40x40.
- Randomly cropping back to the size of 32x32.
- Randomly flipping the training images horizontally.
- Standardizing the train and validation sets to be of a zero-mean and a unit variance.

**Operations and cells.** We select from the operations mentioned in 4.1, with a stride of 1 for all of the connections within a cell but for the reduction cells' connections to the previous cells, which are with a stride of 2. Convolutional layers are padded so that the spatial resolution is kept. The operations are applied in the order of ReLU-Conv-BN. Following [43],[30], depthwise separable convolutions are always applied twice. The cell's output is a 1x1 convolutional layer applied on all of the cells' four intermediate nodes' outputs concatenated, such that the number of channels is

preserved. In CIFAR-10, the search lasts up to 0.2 days on NVIDIA GTX 1080Ti GPU.

**The annealing schedule.** We use the exponential decay annealing schedule as described in Algorithm 1 when setting the annealing schedule as in 4 with  $(T_0, \beta, \tau) = (1.6, 0.95, 1)$ . It was selected for obtaining a final temperature of 0.1 and 5 epochs of grace-cycles.

**Alternate optimization.** For a fair comparison, we use the exact training settings from [11]. We use the Adam optimizer [18] for the architecture weights optimization with momentum parameters of (0.5, 0.999) and a fixed learning rate of  $10^{-3}$ . For the network weights optimization, we use SGD [33] with a momentum of 0.9 as the learning rate is following a cosine annealing schedule [25] with an initial value of 0.025.

### 6.2.2 Training details

**CIFAR-10.** The training architecture consists of 20 cells stacking up: 18 normal cells and 2 reduction cells, located at the 1/3 and 2/3 of the total network depth respectively. The normal cells start with 36 channels, where we double the number of channels after each reduction cell. We train the network for 600 epochs with a batch size of 96. We use the SGD optimizer [33] with a momentum of 0.9, following a cosine annealing learning rate [25] with an initial value of 0.025. We apply a weight decay of  $3 \cdot 10^{-3}$  and a norm gradient clipping at 5. We add an auxiliary loss [35] after the last reduction cell with a weight of 0.4. In addition to data pre-processing, we use cutout augmentations [7] with a length of 16 and a drop-path regularization [21] with a probability of 0.2. For our extended training (ET) mode, we train a network with 44 initial channels for 1200 epochs, with AutoAugment augmentation scheme. Other parameters remains the same.

**ImageNet.** Our training architecture starts with stem cells that reduce the input image resolution from 224 to 56 (3 **reductions**), similar to MobileNet-V1 [14]. We then stack 14 cells: 12 normal cells and 2 reduction cells. The reduction cells are placed after the fourth and eighth normal cells. The normal cells start with 50 channels, as the number of channels is doubled after each reduction cell. The network contains 4.29 million parameters in total. We train the network on 2 GPUs for 250 epochs with a batch size of 192. We use the SGD optimizer [33] with a momentum of 0.9, following an exponential learning rate schedule with an initial value of 0.1, a decay period of 1 epoch and a decay rate of 0.97. We apply a weight decay of  $3 \cdot 10^{-4}$  and a norm gradient clipping at 5. We add an auxiliary loss after the last reduction cell with the weight of 0.4 and a label smoothing [32] of 0.1. During training, we normalize the input image and crop it with a random cropping factor in the range of 0.08 to 1. In addition, color augmentations and randomly horizon-

tal flipping are applied. During testing, we resize the input image to the size of 256x256 and applying a fixed central crop to the size of 224x224.

**Additional datasets.** Our additional classification datasets consist of CINIC-10 [5], CIFAR-100 [36], FREIBURG [17], SVHN [27] and FashionMNIST [38]. Their training scheme was similar to the one used for CIFAR-10, described at 6.2.2, with some minor adjustments and modifications. For the FREIBURG dataset, we resized the original images from 256x256 to 64x64. For CINIC-10, we were training for 400 epochs instead of 600, since this dataset is much larger than CIFAR-10. For the SVHN and CIFAR-100 datasets, we added learned augmentations [4] to our training scheme. Note that for each of those datasets, all of the cells were trained with exactly the same network architecture and hyper-parameters, unlike our ImageNet comparison at 4.3, where each cell was embedded into a different architecture and trained with a completely different scheme.